Femtosecond Laser Machined Micro-Structured Fiber Bragg Grating for Simultaneous Temperature and Force Measurements

Gabriele Marchi, Valentin Stephan, Franz J. Dutz, Barbara Hopf, Leonhard Polz, Heinz P. Huber, and Johannes Roths

***Abstract*—A new fabrication method for a locally micro-structured fiber Bragg grating (LMFBG) is proposed and demonstrated. With this new type of LMFBG, simultaneous sensing of compressive force and temperature is possible. The LMFBG consists of a circumferential groove of $\sim$86 μm length and $\sim$27 μm depth in the middle of a type I FBG. Direct femtosecond (*fs*) laser ablation was applied to manufacture the groove with constant depth and steep side walls. Axial compressive force acting on the LMFBG results in the occurrence of a pass band in the reflection spectrum due to a stress-induced phase shift in the structured part of the LMFBG. Temperature changes instead induce shifts of the whole spectrum without influencing its shape. A theoretical model that can describe the LMFBG reflection spectra is presented. It consists of a product of three transfer matrices for uniform FBGs with external force, temperature, and the optical power used to interrogate the LMFBG as free parameters. The model-based theoretical line shapes showed very good agreements with measured LMFBG spectra at various force and temperature values in the ranges of 5–45 °C and 0 to –1.44 N. The ability to describe the LMFGB as a combination of three uniform FBGs is due to the precise shape of the engraved structure which is a unique feature of *fs* laser machined LMFBGs. The difference between the LMFBG-based force and temperature values and the reference values are $<$0.03 N for force and $<$2.0 K for temperature.**

***Index Terms*—Fiber Bragg grating, *fs* laser machining, temperature-force sensor.**

I. Introduction

FIBER Bragg gratings (FBGs) have found many applications e.g. in structure monitoring, industrial process monitoring and medicine. When compared to electrical sensors, they offer specific advantages in terms of sensor size, multiplexing capability, and immunity to electromagnetic interference. The measurands mostly addressed by FBG-based sensors are mechanical strain and temperature. Force measurements are generally closely related to strain measurements, because typically force is applied to a spring element, for example a cantilever, and its deformation is measured by a sensor element that is attached to the spring element. When space is constrained and small forces are to be measured, the glass fiber itself can be deployed as the spring element of the fiber-optic force sensor. In addition to the above mentioned advantages, the chemical inertness and the electrical passivity of FBG-based force sensors make them in particular suited for biological and medical applications [1], [2].

Recently, some of the authors proposed a fiber-based indentation system for early diagnosis of osteoarthritis which is intended to be deployed *in vivo* during an endoscopic treatment [3]. The key element is an optical fiber including an FBG that is located close to the fiber's cleaved end. The FBG is used to acquire compressive strain when the fiber gets pressed onto the cartilage. The fiber acts as the spring element and the force developed by the cartilage at a given indentation depth is the quantity that is used to characterize the cartilage. The required precision of the force sensing makes a temperature-force discrimination necessary, which is almost always the case in real-world deployments of FBGs.

A variety of schemes for single element temperature and force (or strain) discrimination have been proposed for FBG sensors [4]. They mainly rely on acquiring two spectral quantities that show different sensitivities to temperature and force (strain). Assuming linear dependencies the sensor response is usually described by a sensitivity matrix that has to be inverted to calculate the measurands [5], [6].

For the above mentioned application, all these discrimination schemes show some drawbacks. For example, a dual-wavelength approach [7] is complex to interrogate or the techniques based on FBGs at different diameters of the sensor fiber, which were realized by etching, tapering, or splicing [8]–[12] are relatively long (10–20 mm) and not suited for compressive strain because they tend to buckle.

In locally micro-structured fiber Bragg gratings (LMFBG) the hosting optical fiber is locally changed within the axial extension of the FBG by treatments typically applied after FBG inscription [13]. These treatments include etching and/or thermal processing and lead to a transmission peak within the stopband of an FBG. LMFBGs are mainly intended as filter devices for telecommunication applications and for refractive index sensing. For example, Cusano *et al*. [14] reported a technique based on electric arc discharge for tailoring the spectral properties of LMFBGs. These treatments include a thermal erasure of the refractive index modulation and a tapering of the fiber by localized heating of the fiber [14]. This induces a distributed phase shift within the grating and due to the reduced diameter in the tapered region the phase shift depends on axial strain. Cusano *et al*. have already pointed out that the wavelength of the transmission

Manuscript received February 12, 2016; revised March 30, 2016; accepted May 3, 2016. Date of publication May 11, 2016; date of current version September 22, 2016. This work was supported by the Deutsche Forschungsgemeinschaft under Grant RO 4145/4-1.

The authors are with the University of Applied Sciences, Munich 80335, Germany (e-mail: marchi@hm.edu; valentin.stephan@hm.edu; franz_josef.dutz@hm.edu; barbara.hopf@hm.edu; leonhard.polz@hm.edu; heinz.huber@hm.edu; roths@hm.edu).

Color versions of one or more of the figures in this paper are available online at http://ieeexplore.ieee.org.

Digital Object Identifier 10.1109/JLT.2016.2567779

peak has a larger strain sensitivity than the Bragg wavelength of the pristine fiber and that temperature self-referenced strain measurements are possible by evaluating the difference of the wavelength of the transmission peak and the wavelength of one edge of the FBG stop band [14].

It has been shown recently that *fs* laser micromachining is a powerful tool for tailoring fiber optic sensor elements [15]. Most of these activities are devoted to the formation of in-fiber micro-slots [16], Fabry–Perot structures [17], cantilevers [18] or for activating the surface of the cladding for an improved adhesion of sensitive coatings [19].

In this paper we present a new type of LMFBG that is fabricated by *fs* laser micromachining. With this technique a small circumferential ditch of $\sim$86 μm length and $\sim$27 μm depth in the middle of a $\sim$3 mm long FBG was ablated by *fs* laser treatment. The advantages of this technique are flexibility, precision, and reproducibility when compared to other techniques. Additionally, it allows fabrication of much smaller structures with steeper boundaries, which is essential for many sensor applications of LMFBGs including the above mentioned compressive force sensing. The sensor fiber is guided in a sleeve, so buckling of the fiber section with reduced diameter is suppressed because it is too short. The precise shape of the structure with steep borders between the structured and unstructured parts of the LMFBG allows a good theoretical description of its spectral response with a relative simple sensor model. It consists of three uniform FBGs describing the structured part and the sub-gratings on its left and right hand side. All necessary model parameters can be deduced from experimental characterizations of the pristine FBG and of the LMFBG. Temperature and force dependencies are incorporated into the model resulting in a model-based representation of the complete spectrum of the LMFBG. At constant force temperature changes shift the whole spectrum and have no influence on the shape of the spectrum. Force changes induce both; they shift the whole spectrum and induce a transmission dip in the pristine spectrum that shifts from longer to smaller wavelengths when the compressive force is increased. By fitting the model-based spectrum with temperature and force as free parameters, both values can be determined simultaneously. To our knowledge, this represents a new data evaluation strategy for multi-parameter FBG sensing.

II. Theory

In Fig. 1(a) scheme of the LMFBG is given. The fiber diameters in the left and right sections of the LMFBG $D_l = D_r = 125\,\mu$m are equal. The diameter $D_{str} = 71\,\mu$m of the central *fs* laser machined section of the LMFBG is reduced but still much larger than the mode field diameter. When no stress or temperature changes occur, the effective refractive index n^0_{eff}, the modulation amplitude δn^0_{AC}, and the period of the grating Λ^0 are assumed to be the same in each section. It is assumed that the LMFBG is free of transversal stress and that there is no temperature gradient along the LMFBG. Using transfer matrix theory [20] the LMFBG is modelled as a combination of three uniform FBGs, representing the left and right unmodified sections of the fiber and the central *fs* laser engraved structure. The parameters referring to each section will be indicated by the subscripts $i =$ *l*, *str* or *r* respectively. The complete LMFBG is described by a transfer matrix, T_{LMFBG}, that is given as the product of three transfer matrices $T_{\rm i}$, each representing a uniform FBG,

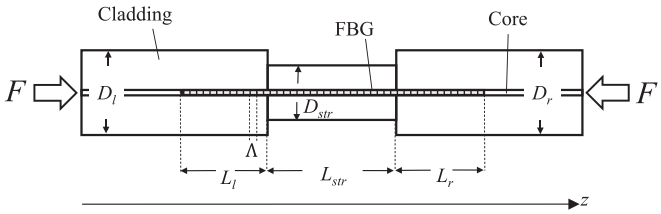

Fig. 1. Scheme of a LMFBG obtained by engraving a circumferential groove in the central part of a FBG.

$$T_{LMFBG} = \prod_i T_i = T_l(\kappa_l, \delta_{d_l})\; T_{str}(\kappa_{str}, \delta_{d_{str}})\; T_r(\kappa_r, \delta_{d_r}). \tag{1}$$

The coupled mode theory [21] provides coupling equations for a uniform grating which are characterized by the so called "AC" coupling coefficient κ and the "DC" self-coupling coefficient δ_d. So, each uniform section of the LMFBG can be described by the parameters κ_i and δ_{d_i}. For the *i*th section these parameters can be expressed as functions of signal wavelength λ, strain ε_i, and temperature T, as

$$\delta_{\rm d_i} = 2\pi \left[\frac{n_{\mathit{eff}_i}(\varepsilon_i, T)}{\lambda} - \frac{1}{2\Lambda_i(\varepsilon_i, T)} \right], \tag{2}$$

$$\kappa_i = \frac{\pi}{\lambda} \delta n_{AC_i}(\varepsilon_i, T), \tag{3}$$

where n_{eff_i} is the effective refraction index of the mode, δn_{AC_i} is the modulation amplitude of the refraction index and Λ_i is the period of the grating in each section. Each section of the LMFBG can be described as a uniform grating with a transfer matrix T_i, which is given by [20] (4) as shown at the bottom of the page, with

$$\mu_i^2 = \kappa_i^2 - \delta_{d_i}^2. \tag{5}$$

If axial compressive force F is applied the structured section will experience a higher axial compressive strain than the left and right sub-FBGs due to its reduced diameter. Following

$$T_i(\kappa_i, \delta_{d_i}) = \begin{pmatrix} \cosh(L_i\mu_i) - i\dfrac{\delta_{\rm d_i}\sinh(L_i\mu_i)}{\mu_i} & -i\dfrac{\kappa_i \sinh(L_i\mu_i)}{\mu_i} \\ i\dfrac{\kappa_i \sinh(L_i\mu_i)}{\mu_i} & \cosh(L_i\mu_i) + i\dfrac{\delta_{\rm d_i}\sinh(L_i\mu_i)}{\mu_i} \end{pmatrix} \tag{4}$$

Young's law, the strain in each section, ε_i, can be described by

$$\varepsilon_i = \frac{4F}{\pi D_i^2 E_i}. \tag{6}$$

E_i is the effective Young's modulus which is here allowed to have individual values in each section. The fiber employed here has an inner and outer cladding with different material compositions and Young's moduli (see Section III). Changing the diameter of the outer cladding by laser machining will change the ratio of the cross sections of the inner- and outer cladding and thus different effective Young's moduli in the structured and unstructured sections are expected.

The dependencies of the parameters κ_i and δ_{d_i} on strain ε_i and temperature changes ΔT are given by (2) and (3) and the following equations, using linear approaches for the thermooptic and optoelastic effects [22],

$$\delta n_{AC_i}(\varepsilon_i, \Delta T) = (1 - p_e\varepsilon_i + \alpha_n \Delta T)\delta n^0_{AC}, \tag{7}$$

$$n_{eff_i}(\varepsilon_i, \Delta T) = (1 - p_e\varepsilon_i + \alpha_n \Delta T) n^0_{eff}, \tag{8}$$

$$L_i(\varepsilon_i, \Delta T) = (1 + \varepsilon_i + \alpha_\Lambda \Delta T) L^0_i, \tag{9}$$

$$\Lambda_i(\varepsilon_i, \Delta T) = (1 + \varepsilon_i + \alpha_\Lambda \Delta T)\Lambda^0. \tag{10}$$

Here the superscript "0" indicates the quantities without stress at reference temperature. The parameter p_e is the opto-elastic coefficient, and α_n and α_Λ are the thermo-optic and the thermal expansion coefficient of the fiber. It is assumed here that these parameters don't change due to the structuring of the fiber.

The period of the grating Λ^0 without thermal and mechanical load is given by [22],

$$\Lambda^0 = \Lambda_{\mathrm{PM}}/2, \tag{11}$$

where Λ_{PM} is the period of the phase mask used for inscribing the pristine FBG. The quantities n^0_{eff}, n^0_{AC} can be deduced from the reflection spectrum of the pristine grating, as shown in Section III. The lengths of the left, L^0_l, and right, L^0_r, sub-FBGs are determined by the length, L^0_{str}, and the position of the *fs* laser machined structure within the pristine FBG. The constraint $L^0_l + L^0_{str} + L^0_r = L^0$ has to be fulfilled, where $L^0 = 3.0$ mm is the length of the pristine FBG which is known from the inscription procedure.

Using (1)–(10) the transfer matrix of the LMFBG can be expressed as a function of force F and temperature change ΔT,

$$T_{LMFBG}(F, \Delta T) = \begin{pmatrix} T_{11}^{LMFBG}(F, \Delta T) & T_{12}^{LMFBG}(F, \Delta T) \\ T_{21}^{LMFBG}(F, \Delta T) & T_{22}^{LMFBG}(F, \Delta T) \end{pmatrix}. \tag{12}$$

The power reflectivity spectrum $|r(\lambda)|^2$ is the quantity that is measured if the LMFBG is operated in reflection mode. It is given by the ratio of the elements in the first column of $T_{LMFBG}(F, \Delta T)$ [20],

$$|r(\lambda, F, \Delta T)|^2 = \left| \frac{T_{11}^{LMFBG}(F, \Delta T)}{T_{21}^{LMFBG}(F, \Delta T)} \right|^2. \tag{13}$$

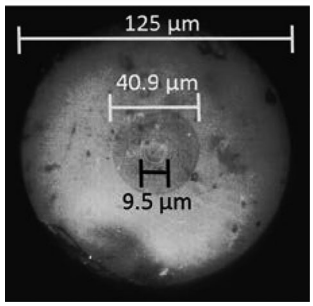

Fig. 2. Cross section of the photosensitive fiber (Nufern GF1B). Clearly visible are the core (0–9.5 μm diameter), the inner cladding (9.5–40.9 μm diameter), and the outer cladding (40.9–125 μm diameter).

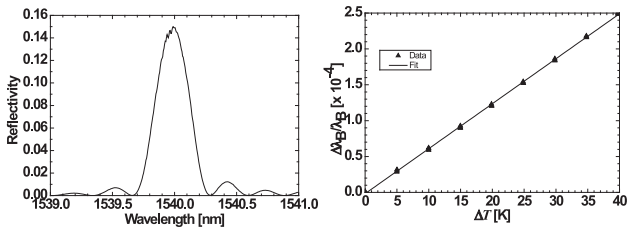

(a) (b)

Fig. 3. (a) Reflectivity spectrum of the pristine FBG. (b) Relative Bragg wavelength shift as a function of temperature change, ΔT. The function fitted was $\Delta\lambda_B/\lambda_B = \alpha_T \Delta T$ with $\alpha_T = 6.21 \times 10^{-6}\, K^{-1}$.

III. Fabrication of the LMFBG

The LMFBG was produced by *fs* laser machining of a type I FBG that had been inscribed with a phase mask and a 248 nm exciplex laser in a photosensitive fiber (Nufern GF1B). As can be seen in Fig. 2 the GF1B fiber consists of a core, an inner and an outer cladding. According to manufacturer's information the core is doped with *Ge* and *F*, the inner cladding is doped with *Ge*, *P* and *F* whereas the outer cladding is pure fused silica. It can be expected that doping fused silica leads to a reduction of its Young's modulus [23]. Thus the elastic behavior of the fiber has to be described with an effective Young's modulus that takes into account the contributions of all three parts of the fiber.

Before machining the fiber, a series of preliminary measurements were performed to determine several parameters that were needed for the theoretical model. The reflectivity spectrum of the pristine FBG was acquired at reference temperature (i.e. at $\Delta T = 0$) and without mechanical load (Fig. 3(a)). The Bragg wavelength λ_B was obtained by fitting a second order polynomial to the peak of the reflectivity spectrum and λ_{B} was used to determine n^0_{eff} by using the equation $n^0_{eff} = \lambda_B/2\Lambda^0$ [22]. The peak reflectivity $|r_{\max}|^2$ is also taken from the data shown in Fig. 3(a) and gives the amplitude of the refractive index modulation δn^0_{AC} when employing [20]

$$\delta n^0_{AC} = \lambda_B \frac{\sqrt{\operatorname{arctanh} |r_{\max}|^2}}{\pi\, L^0}. \tag{14}$$

Fig. 3(b) shows the measured relative wavelength shift as a function of temperature change of the pristine FBG. An approximately linear relationship with a slope of $\alpha_T = 6.21 \times$

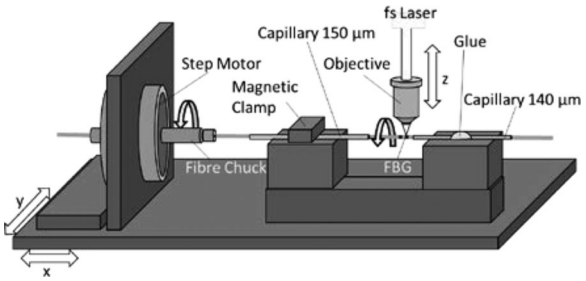

Fig. 4. Schematics of the set-up used for manufacturing the LMFBG.

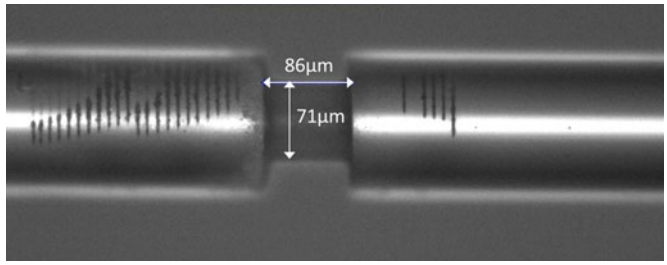

Fig. 5. Microscope picture of a locally micro-structured FBG using *fs* laser machining.

$10^{-6}\mathrm{K}^{-1}$ was found. The slope represents the sum of the coefficient of thermal expansion α_Λ and the thermooptic coefficient α_n, $\alpha_T = \alpha_\Lambda + \alpha_n$. The thermal expansion coefficient is assumed to be $\alpha_\Lambda = 5.5 \times 10^{-7}\mathrm{K}^{-1}$ [24] which results to $\alpha_n = \alpha_T - \alpha_\Lambda = 5.66 \times 10^{-6}\mathrm{K}^{-1}$.

The setup used for manufacturing the LMFBG is shown in Fig. 4. The used *fs* laser source (High-Q femtoREGEN UC) has a wavelength of 1036.3 nm, a pulse rate of 60 kHz and an average power of about 106 mW. The beam was directed by a mirror towards a microscope objective which had a numerical aperture of 0.6, a magnification factor of $32\times$, and a focal length of 6 mm. The calculated focal waist at $1/e^2$intensity and the Rayleigh length were 3.22 μm and 7.89 μm respectively. The focal spot of the laser beam could be adjusted in vertical (z) direction by moving the objective with a translation stage. Two additional translation stages were used for positioning the set-up horizontally in the *xy*-plane. All translation stages were computer controlled and had a precision of about 1 μm. The set-up consisted of a fiber chuck that was mounted on a motor-driven rotation device and two capillaries. The axes of all devices were aligned and the separation between the capillaries was about 1 cm.

The uncoated fibre with the FBG was cleaved about 4 cm behind the FBG. The cleaved end of the fibre was inserted through the fibre chuck, the 150 μm capillary and finally into the 140 μm capillary. The fibre was slided into the setup until the FBG was positioned just outside the entrance of the 140 μm capillary (see Fig. 4). Then the fibre chuck was tightened to retain the fibre.

The laser spot was focussed on the surface at the top of the fibre and laser power was applied meanwhile the fibre was continuously rotated. The rotating speed was chosen to get a pulse overlap of 99%. After a full rotation was completed the spot was shifted for 3 μm along the *x*-axis and was hold there until a new rotation was completed. The process went on until an axial length of 86 μm was scanned. Then the objective was lowered by 1 μm, the fiber was positioned at its initial *x*-position and another scan was initiated. The desired depth of the structure fixed the number of scans to be done. A microscope picture of the LMFBG is depicted in Fig. 5. The structure showed a cylindrical symmetry and steep boundaries of the circumferential groove. An average diameter of $D_{str} = 71$ μm and an average width of $D_{str} = 86.6$ μm were obtained with a maximum deviation of ± 2 μm from the average for both radius and width.

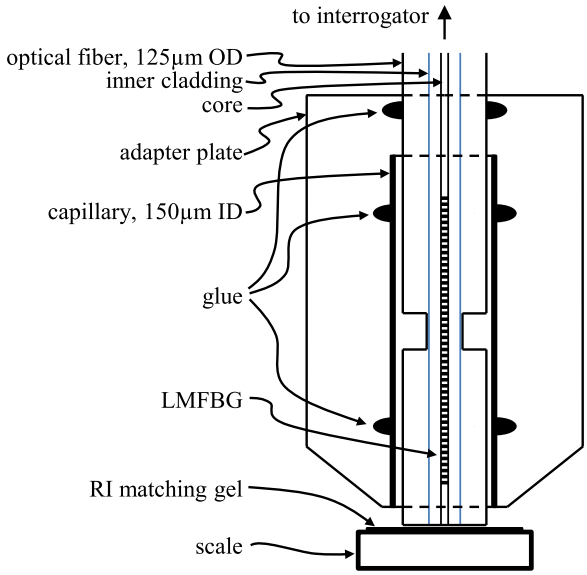

Fig. 6. Set-up for investigating the LMFBG spectra under variable compressive axial force and temperature.

IV. Experiment

To investigate the decoupling of compressive force and temperature the LMFBG was inserted into a capillary of ~70 mm length and 150 μm inner diameter (see Fig. 6). The fiber was aligned so that its cleaved end protruded about 2 mm out of the lower end of the capillary. In this position the capillary and the fiber were fixed on an aluminum plate with several dots of glue (see Fig. 6). The capillary was necessary to avoid bending when the sensor fiber was loaded with compressive force. The sensor head was mounted on a vertically oriented micrometer-driven translation stage. A scale (Ohaus Scout Pro) with 0.1 g resolution was positioned under the tip of the sensor head. This setup was placed inside a temperature chamber (Vötsch VCL4010). The spectral response of the sensor was obtained with a sm125 interrogator (Micron Optics) that was located outside of the temperature chamber.

Measurements were performed at five temperatures between 5 and 45 °C. After the system had reached thermal equilibrium the micrometer stage was manually lowered so that the tip of the sensor fiber was pressed on the scale and different force levels were applied to the structure. At each force value the spectra of the LMFBG and the actual temperature of the climate chamber were recorded. The access to the micrometer drive was possible

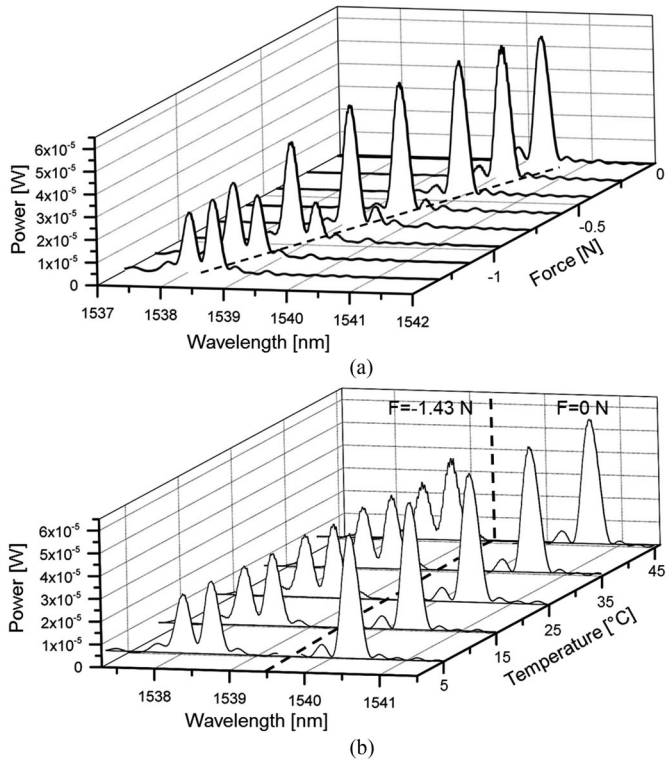

Fig. 7. (a) Spectra at different values of compressive force at a temperature of 5 °C. The dashed line indicates the trajectory of the minimum of the pass band dip. The value of the force is negative to indicate compression. (b) Spectra at different temperatures when no compressive force was applied and when a force of $F = -1.43$ N was applied.

due to a small side opening in the wall of the chamber. The manual access to the setup inside the climate chamber induced inevitable temperature variations which were up to 2.4 °C during a force-spectra measurement series.

In Fig. 7(a) the spectra recorded at different compressive force values at 5 °C are shown as examples. Due to different phase shifts in the three sections of the LMFBG, a transmission band sweeps across the reflection spectrum from higher to lower wavelengths if the compressive force is increased. The shift of the minimum wavelength of the transmission band was found to be proportional to force with a slope of 1.63 ± 0.04 nm/N. This represents a 18% higher force sensitivity relative to an unstructured FBG in the same fiber [25]. At the maximum compressive force applied in this experiment (∼–1.43 N) the transmission dip was almost in the middle of the pristine FBG spectrum. If the compressive force is further increased the transmission dip will be expected to move further towards lower wavelengths. In Fig. 7(b) the spectra at different temperatures are given for two values of applied force, namely 0 and –1.43 N as examples. Almost no changes in the spectral distribution were visible as a consequence of temperature changes but a shift of the whole spectrum towards larger wavelengths was observed. This was also found at all other temperature and force values investigated. At constant force the shift of the wavelength of the largest peak in the LMFBG spectra with temperature was found to be independent of the applied force and gave for all measurement series performed in this study an average value of 9.7 ± 0.3 pm/K.

TABLE I
LIST OF THE SENSOR PARAMETERS AND THEIR VALUES USED IN THE THEORETICAL MODEL OF THE LMFBG

Parameter		Left FBG	Structure	Right FBG
Grating length	L_i^0	1.1 mm*	87 μm	1.9 mm*
Fibre diameter	D_i	125 μm	71 μm	125 μm
Young's modulus	E_i	73.1 GPa	51 GPa*	73.1 GPa
Effective refraction Index	n_{eff}^0	1.44788		
Period	Λ^0	0.5318 μm		
Index modulation	δn_{AC}^0	6.7×10^{-5}		
Force offset ($m = 0$ g)	F^0	0.29 N*		
Opto-elastic coefficient	p_e	0.211		
Thermal expansion coefficient	α_Λ	$0.55 \times 10^{-6}\,\mathrm{K}^{-1}$		
Thermo-optical coefficient	α_n	$5.66 \times 10^{-6}\,\mathrm{K}^{-1}$		

The subscript "$*$" denotes values obtained by a calibration measurement as described in Section V.

V. SPECTRA EVALUATION AND DISCUSSION

For employing the theoretical model described in Section II a complete set of model parameter had to be found. Table I gives an overview of the values of the model parameters used. The determination of the values of the parameters α_n, Λ^0, n_{eff}^0, δn_{AC}^0, L^0, L_{str}^0 and D_{str} have already been addressed in the previous sections. The elasto-optical coefficient $p_e = 0.211$ and the Young's modulus of the GF1B fiber, $E = 73.1$ GPa, were derived from Jülich *et al*. [26]. The model parameters L_l^0 and E_{str} were determined by calibration measurements as described below. For this purpose two spectra (taken at $T = 5\,^\circ$C and at $F = 0$ N and $F = -1.43$ N force) from the data set aquired during the experiments described in Section IV served as calibration data. These experimental data $P(\lambda)$ are depicted in Fig. 8. It turned out that it was not possible to describe the spectrum shown in Fig. 8(a) with a theoretical function, given by

$$P_{LMFBG}(\lambda) = P^0 \ |r(\lambda)|^2 . \tag{15}$$

P^0 is a fit parameter that accounts for the optical power of the interrogator, and $|r(\lambda)|^2$ is the model-based power-reflectivity spectrum (13) with fixed parameters $T = 5\,^\circ$C and $F = 0$ N and with E_{str} and L_l^0 as the free parameters. It was only possible to fit this experimental spectrum by replacing the force with $\tilde{F} = F + F^0$ and F^0 was allowed to be a fourth free parameter for the fit. This becomes obvious when this spectrum is compared to the spectrum of the pristine FBG (Fig. 3(a)). The pristine spectrum is fairly symmetric but after machining the spectrum (Fig. 8(a)) becomes unsymmetric and shows a higher side lobe at the lower wavelength side. F^0 can be interpreted as an effective offset force, which is present in the structured part of the LMFBG resulting in a modification of (6) for the structured part,

$$\varepsilon_{str} = \frac{4\left(F - F^0\right)}{\pi D_{str}^2 E_{str}}. \tag{16}$$

Therefore, the four free model variables P^0, E_{str}, L_l^0 and F^0 were varied iteratively until the calculated spectra showed good agreement with both experimental spectra as shown in Fig. 8(a) and (b). The Young's modulus of the structure found by this

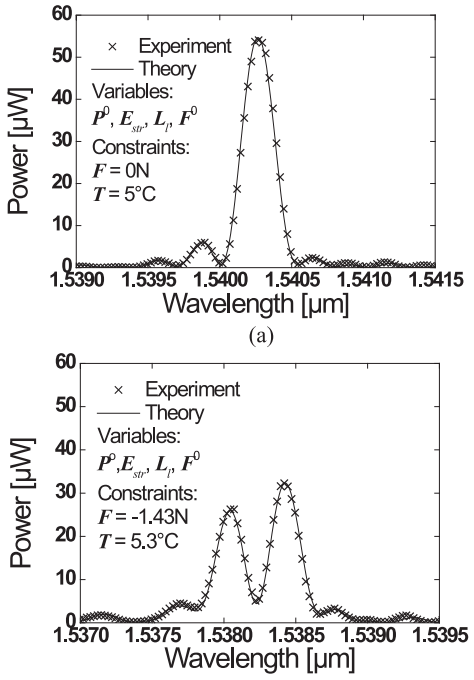

Fig. 8. Spectra measured at (a) $F = 0$ N and $T = 5.0$ °C and (b) $F = -1.43$ N and $T = 5.3$ °C together with corresponding fits of theoretical line shapes. Temperature and force are fixed parameters and P^0, E_{str}, L_l and F^0 are free parameters. The fits are used to retrieve the parameters $E_{str} = 51$ GPa, $L_1 = 1.1$ mm and $F^0 = 0.29$ N.

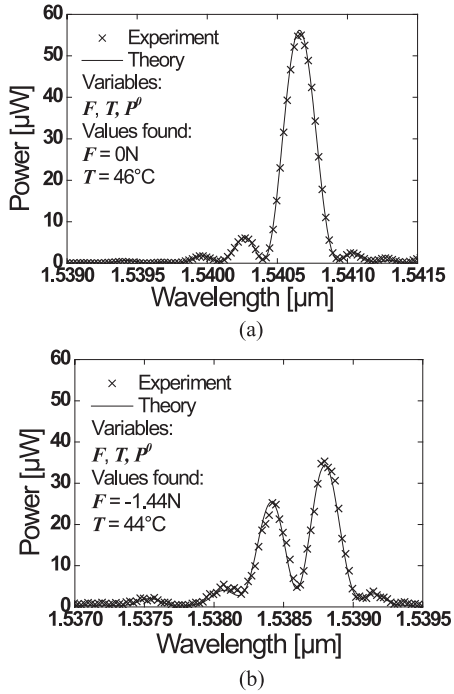

Fig. 9. Spectra measured at (a) $F = 0$ N and $T = 45$ °C and (b) $F = -1.42$ N and $T = 42.6$ °C together with corresponding fits of theoretical line shapes as examples. For these fits the parameters E_{str}, L_l and F^0 are fixed and P^0, temperature and force are free parameters. The fit values of temperature and force agree well with the corresponding reference values.

procedure was $E_{str} = 51$ GPa. This is a lower value than the moduli of the left and right FBG and can be attributed to the influence of the highly doped inner cladding. The grating length of the left sub-FBG was found to be $L_l^0 = 1.1$ mm, resulting in a length of $L_r^0 = L^0 - L_{str}^0 - L_l^0 = 1.9$ mm for the right sub-FBG. This means that the structure was located 0.4 mm from the middle of the pristine FBG. The offset force was found to be $F^0 = 0.29$ N. The occurrence of a positive offset force can be explained with regard to in-frozen axial stresses. The in-frozen axial stresses originate from the fiber drawing process, since the highly doped inner cladding and core have lower viscosity than the outer cladding at high temperatures. Hence, in the pristine fiber the inner cladding is under a compressive and the outer cladding under tensile axial strain [27]. During the micromachining process a large part of the outer cladding is removed. This allows the inner cladding and the core to expand which shows up here as an effective offset-force.

Having all model parameters fixed, the model was used to retrieve temperature and force values from all remaining spectra obtained during the experiments described in Section IV. To extract the temperature and force from a spectrum, the same fit procedure as described above was performed but now leaving only P^0, F and T as free parameters. In Fig. 9 the calculated and recorded spectra for two different forces at about 45 °C are shown as examples. The excellent agreement between the theoretical and the experimental spectra can be seen.

Fig. 10 shows the values of force and temperature obtained by the LMFBG and the reference values measured with the

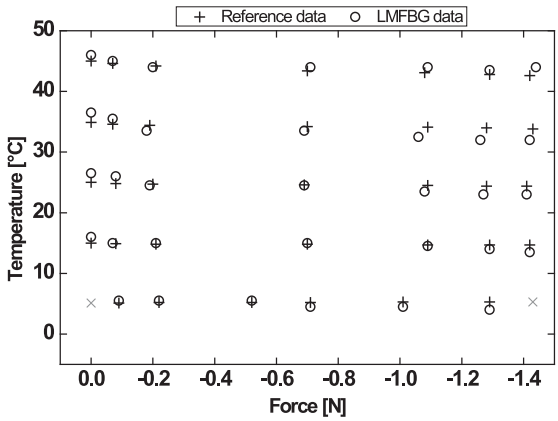

Fig. 10. Comparison of the LMFBG-based force and temperature data with the reference values. The gray marks at (5 °C; 0 N) and (5 °C, −1.43 N) denote the measurements used for calibrating the LMFBG.

thermometer and the scale. A good agreement between the LMFBG-based and the reference values of force and temperature is evident. The difference between the reference and the LMFBG-based values show are < 0.03 N for force and < 2.0 °C for temperature. The relatively low precision in the temperature determination is mainly attributed to the large temperature variations during the experiments as a consequence of the poor temperature stability resulting from the open side hole in the climate chamber that was needed for having manual access to the translation stage.

By increasing the diameter and reducing the length of the structured region, the force measurement range can be extended.

Furthermore, improved measurement precision can be expected with an optimized LMFBG. Using a stronger pristine FBG with higher δn_{AC} the LMFBG spectra will have steeper slopes and a very narrow pass band. Therewith, reduced uncertainties of the fitting parameters can be expected. The force sensitivity of the pass band scales linearly with the length of the structure, L^0_{str}, and inversely with the cross section of the fiber ($\propto D^{-2}_{str}$. Thus, the precision of the force measurement can be enhanced by extending the length and reducing the diameter of the structured section (at the cost of a reduced force measurement range). However, this approach is limited because it increases the tendency for buckling under compressive strain and reduces the mechanical stability of the fiber. Generally, the mechanical stability limits the applicability of *fs* laser machined LMFBGs for tensile strain sensing. It has been shown here that operating the LMFBG within a sleeve provides a robust, reliable and minaturized sensor mounting for simultaneous compressive force and temperature sensing.

VI. Conclusion

A new method for producing LMFBGs by means of *fs* laser machining is reported. The LMFBG consists of a circumferential groove of $\sim$86 μm length and $\sim$27 μm depth in the middle of a 3.0 mm long type I FBG. *Fs* laser machining allowed the realization of steep boundaries of the groove. A modular model of the LMFBG based on a product of three transfer matrices of uniform FBGs was developed. All model parameters were determined experimentally by characterization measurements of the pristine FBG and the LMFBG leaving only the power of the interrogator unit, the force and temperature as free parameters. This model is capable of fitting the experimental spectra of the LMFBG with very good agreement for different compressive forces and at different temperatures. Comparison measurements in the temperature range from 5 to 45 °C and in a force range from 0 to 45 N show differences between the LFMBG-based and reference values of $<$0.03 N for force and $<$2.0 K for temperature.

Acknowledgment

The authors would like to thank R. Kuttler, M. Domke, S. Rapp, J. Winter, and R. Moser for their invaluable support during the experiments.

References

[1] P. Roriz, L. Carvalho, O. Frazão, J. L. Santos, and J. A. Simões, "From conventional sensors to fibre optic sensors for strain and force measurements in biomechanics applications: A review," *J. Biomech.*, vol. 47, pp. 1251–1261, 2014.

[2] A. Abushagur, N. Arsad, M. Reaz, and A. Bakar, "Advances in bio-tactile sensors for minimally invasive surgery using the fibre Bragg grating force sensor technique: A survey," *Sensors*, vol. 14, pp. 6633–6665, 2014.

[3] G. Marchi, M. Jost, A. Steinkopff, C. Prein, A. Aszodi, H. Clausen-Schaumann, and J. Roths, "All optical indentation probe for endoscopic diagnosis of ostheoarthritis," *Proc. SPIE*, vol. 9529, 2015, Art. no. 95291A.

[4] O. Frazão, L. A. Ferreira, F. M. Araújo, and J. L. Santos, "Applications of fiber optic grating technology to multi-parameter measurement," *Fiber Integr. Opt.*, vol. 24, pp. 227–244, 2005.

[5] M. G. Xu, J. L. Archambault, L. Reekie, and J. P. Dakin, "Simultaneous measurement of strain and temperature using fibre grating sensors," Proc. presented at the 10th Int. Conf. Optical Fibre Sensors, Glasgow, U.K., 1994.

[6] A. D. Kersey, M. A. Davis, H. J. Patrick, M. LeBlanc, K. P. Koo, C. G. Askins, M. A. Putnam, and E. J. Friebele, "Fiber grating sensors," *J. Lightw. Technol.*, vol. 15, no. 8, pp. 1442–1463, Aug. 1997.

[7] M. G. Xu, J. L. Archambault, L. Reekie, and J. P. Dakin, "Discrimination between strain and temperature effects using dual-wavelength fibre grating sensors," *Electron. Lett.*, vol. 30, pp. 1085–1087, 1994.

[8] M. G. Xu, L. Dong, L. Reekie, J. A. Tucknott, and J. L. Cruz, "Temperature-independent strain sensor using a chirped Bragg grating in a tapered optical fibre," *Electron. Lett.*, vol. 31, pp. 823–825, 1995.

[9] O. Frazão, M. Melo, P. V. S. Marques, and J. L. Santos, "Chirped Bragg grating fabricated in fused fibre taper for strain–temperature discrimination," *Meas. Sci. Technol.*, vol. 16, pp. 984–988, 2005.

[10] W. Zhou, C.-L. Zhao, X. Dong, S. Zhang, C. C. Chan, and P. Shum, "Simultaneous measurement of force and temperature based on a half corroded FBG," *Microw. Opt. Technol. Lett.*, vol. 52, pp. 2020–2023, 2010.

[11] O. Frazão, L. Marques, J. M. Marques, J. M. Baptista, and J. L. Santos, "Simple sensing head geometry using fibre Bragg gratings for strain–temperature discrimination," *Opt. Commun.*, vol. 279, pp. 68–71, 2007.

[12] S. W. James, M. L. Dockney, and R. P. Tatam, "Simultaneous independent temperature and strain measurement using in-fibre Bragg grating sensors," *Electron. Lett.*, vol. 32, pp. 1133–1134, 1996.

[13] A. Cusano, D. Paladino, and A. Iadicicco, "Microstructured fiber Bragg gratings," *J. Lightw. Technol.*, vol. 27, no. 11, 1663–1697, Jun. 2009.

[14] A. Cusano, A. Iadicicco, D. Paladino, S. Campopiano, and A. Cutolo, "Photonic band-gap engineering in UV fiber gratings by the arc discharge technique," *Opt. Express*, vol. 16, pp. 15332–15342, 2008.

[15] Y.-J. Rao and Z.-L. Ran, "Optic fiber sensors fabricated by laser-micromachining," *Opt. Fiber Technol.*, vol. 19, pp. 808–821, 2013.

[16] K. Zhou, Y. Lai, X. Chen, K. Sugden, L. Zhang, and I. Bennion, "A refractometer based on a micro-slot in a fiber Bragg grating formed by chemically assisted femtosecond laser processing," *Opt. Express*, vol. 15, pp. 15848–15853, 2007.

[17] Z. L. Ran, Y. J. Rao, W. J. Liu, X. Liao, and K. S. Chiang, "Laser-micromachined Fabry–Perot optical fiber tip sensor for high-resolution temperature-independent measurement of refractive index," *Opt. Express*, vol. 16, pp. 2252–2263, 2008.

[18] F. Albri, A.Y. Li, R. R. J. Maier, W. N. MacPherson, and D. P. Hand, "Laser machining of sensing components on the end of optical fibres," *J. Micromech. Microeng.*, vol. 23, 2013, Art. no. 045021.

[19] Y. Dai, M. Yang, G. Xu, and Y. Yuan, "Magnetic field sensor based on fiber Bragg grating with a spiral microgroove ablated by femtosecond laser," *Opt. Express*, vol. 21, pp. 17386–17391, 2013.

[20] A. Othonos and K. Kalli, *Fiber Bragg Gratings: Fundamentals and Applications in Telecommunications and Sensing*. London, U.K.: Artech House, 1999.

[21] T. Erdogan, "Fiber grating spectra," *J. Lightw. Technol.*, vol. 15, no. 8, pp. 1277–1294, Aug. 1997.

[22] K. O. Hill and G. Meltz, "Fiber Bragg grating technology fundamentals and overview," *J. Lightw. Technol.*, vol. 15, no. 8, pp. 1263–1276, Aug. 1997.

[23] D. Faoite, D. J. Browne, F. R. Chang-Díaz, and K. T. Stanton, "A review of the processing, composition, and temperature-dependent mechanical and thermal properties of dielectric technical ceramics," *J. Mater. Sci.*, vol. 47, pp. 4211–4235, 2011.

[24] R. Roy, A. D. K. Agrawal, and H. A. McKinstry, "Very low thermal expansion coefficient materials," *Annu. Rev. Mater. Sci.*, vol. 19, pp. 59–81, 1989.

[25] J. Roths and F. Jülich, "Determination of strain sensitivity of free fiber Bragg gratings," *Proc. SPIE*, vol. 7003, 2008, Art. no. 700308.

[26] F. Jülich, L. Aulbach, A. Wilfert, P. Kratzer, R. Kuttler, and J. Roths, "Gauge factors of fibre Bragg grating strain sensors in different types of optical fibres," *Meas. Sci. Technol.*, vol. 24, 2013, Art. no. 094007.

[27] A. D. Yablon, "Optical and mechanical effects of frozen-in stresses and strains in optical fibers," *IEEE J. Sel. Topics Quantum Electron.*, vol. 10, no. 2, pp. 300–311, Mar./Apr. 2004.

Authors' biographies not available at the time of publication.